Hindawi
Shock and Vibration
Volume 2019, Article ID 4039862, 9 pages
https://doi.org/10.1155/2019/4039862

Research Article

Operational Deflection Shape Extraction from Broadband Events of an Aircraft Component Using 3D-DIC in Magnified Images

Ángel J. Molina-Viedma,[1] **Elías López-Alba**,[1] **Luis Felipe-Sesé**,[2] **and Francisco A. Díaz**[1]

[1]*Departamento de Ingeniería Mecánica y Minera, Campus Las Lagunillas, Universidad de Jaén, 23004 Jaén, Spain*
[2]*Departamento de Ingeniería Mecánica y Minera, Campus Científico Tecnológico de Linares, Universidad de Jaén, 23700 Linares, Spain*

Correspondence should be addressed to Ángel J. Molina-Viedma; ajmolina@ujaen.es

Received 30 November 2018; Revised 12 February 2019; Accepted 5 March 2019; Published 9 April 2019

Academic Editor: Nuno M. Maia

Recently, many works have shown the capabilities of noninterferometric optical techniques, such as digital image correlation, to characterise modal behaviour. They provide a global insight into the structure or component behaviour which implies massive spatial information, unaffordable by traditional sensor instrumentation. Moreover, phase-based motion magnification (PMM) is a methodology which, based on a sequence of images, magnifies a periodic motion encoded in phase time-domain signals of the complex steerable pyramid filters employed to decompose the images. It provides a powerful tool to interpret deformation. However, the interpretation is just qualitative and should be avoided if out-plane motion is recorded as only one camera is employed. To overcome this issue, 3D digital image correlation (3D-DIC) has been linked with PMM to provide measurements from stereoscopic sets of images, providing full-field displacement maps to magnified images. In this work, the combination of PMM and 3D-DIC has been employed to evaluate the modal behaviour of an aircraft cabin under random excitation. The study was focused on the passenger window area due to its significance to the structural integrity as a discontinuity of the peel. Operational deflection shapes at different resonances were characterised by magnifying a single resonance in the spectrum and then measuring with 3D-DIC. These measurements were validated with those obtained in forced normal mode tests. Motion and displacement videos improved the understanding of the identified resonance deformation. Actually, a relevant behaviour was noticed in the window's frame, a quite narrow area where using traditional sensors would not provide such a detailed 3D information.

1. Introduction

Structural integrity of aircraft is a vital issue. These structures undergo strict controls under severe conditions to provide safety and excellent dynamic performance. Many efforts are taken during design and validation stages in prediction with powerful numerical simulations and expensive, challenging experimental measurements, respectively. Modal parameter inspection is a typical way to detect damage or abnormal behaviour and also to characterise the generated noise inside the cabin. Experimentally, the instrumentation of big structures is usually sparse to prevent the cost increasing. Hence, low spatial resolution provides a rough characterisation regarding mode shapes or even missed due to spatial aliasing. Especially, the resolution is not enough to understand the behaviour of small critical areas. In this sense, full-field optical techniques offer an ultrahigh spatial resolution compared to pointwise methods and, thanks to high speed cameras, represent an interesting alternative for modal identification. Digital image correlation (DIC) [1] is one of the most popular methods due to its robustness, well-developed methodology, and user-friendly commercial

software. But the main advantage over most of the techniques is the possibility of performing 3D measurements by setting up a calibrated stereovision system of two or more cameras. Different studies have explored 3D-DIC for modal identification [2–5]. In a previous work, the authors evaluated the effect of differential pressure on the modal behaviour of aircraft using 3D-DIC [6]. These studies proved the capabilities of the technique to determine full-field mode shapes, avoiding any spatial aliasing.

An interesting methodology recently developed is phase-based motion magnification (PMM). It is a new Eulerian approach to motion processing developed by Wadhwa et al. [7]. It is intended to reveal subtle motion in videos by obtaining a magnified version. The video signals are decomposed using complex steerable pyramid filters [8–10]. This is an overcomplete transform based on complex sinusoids modulated by a Gaussian window function at different spatial scales, orientations, and positions. The time-domain local phase at every spatial scale and orientation of a steerable pyramid, where the motion is encoded, is temporally band-pass filtered and amplified by a magnification factor. When images are reconstructed back, the result is the magnification of the harmonic motion in that frequency band. This method is advantageous over the previous linear amplitude-based Eulerian magnification method [11] since it is possible to achieve larger amplitudes without distortion. Moreover, it provides substantially better noise performance since there is no increment of spatial noise amplitude. This methodology has been employed by Chen et al. to describe operational deflection shapes (ODS) under forced normal mode tests using the edge detection algorithm to highlight the magnified shapes [12]. Sarrafi et al. [13] also employed the edge detection on magnified images for damage detection by noticing changes in natural frequencies and ODSs. PMM has also been employed to develop an autonomous methodology for experimental modal analysis with a little user supervision [14, 15]. Natural frequency and damping are determined from phase signals under random excitation, whereas mode shapes were magnified and highlighted using the edge detection. This methodology has been employed for damage detection localisation using fractal dimension [16].

That is very valuable; however, numerical information or quantifying the motion in terms of displacement is not available. To achieve this, the authors developed a methodology to measure the magnified images using 2D-DIC under sinusoidal excitation to determine displacements in the sensor plane [17]. This demonstrated to be beneficial to provide a full-field measurement to magnified images. In addition, it improved the quality of the ODSs measurement due to the larger motion, considering the typical limitations of DIC for low-amplitude vibrations. Nevertheless, the mentioned phase-based methodologies and also the combination with 2D-DIC employ a system with a single camera. It is only suitable to visualise in-plane motions and, thus, only for 2D displacements. Considering that, the authors evaluated the validity of the measurement on magnified images from a stereoscopic system using 3D-DIC [18]. Under analogous conditions, the obtained ODSs were compared with numerical simulations for a cantilever beam and it was demonstrated that no distortion occurred as a consequence of separate magnification of the images from each camera. This methodology was then performed on a large aeronautical panel where 3D-DIC measurements provided out-of-plane information that could not be assessed by simple visual inspection despite magnification.

In this study, the capabilities of the combination of 3D-DIC and PMM are explored during random excitation to enable multiple mode evaluation in a single test. In a previous study on stereophotogrammetry and magnification in random tests, Poozesh et al. [19] employed 3D-DIC to reveal one low response mode of a simple cantilever beam. Here, the passenger window of a full-scale aircraft demonstrator is evaluated. Multiple modes have been magnified to reveal the shape after a previous identification in a stabilisation diagram. ODSs have been obtained in a full-field manner with negligible presence of noise or other modes. The results have been validated using the mode shapes from forced normal mode tests. Videos of the naked motion and also including the displacement maps allowed an intuitive interpretation of the deformation. That allowed behaviour characterisation of the window frame, what is of significant interest for the structure integrity.

2. Experimental Tests

The methodology for ODSs evaluation using PMM and 3D-DIC was performed in Clean Sky GRA MT2 Cockpit Demonstrator shown in Figure 1. The demonstrator consisted in a cabin fixed to a bulkhead and was fully instrumented to characterise and evaluate the behaviour under different force and environmental conditions. However, these sensors are not employed in this study. This work is focused on a specific part of the demonstrator, the passenger window, highlighted in Figure 1, which involves a discontinuity in the composite peel. Hence, this part plays a critical role in noise generation and keeping the airtightness.

An electrodynamic shaker model LDS V450 was employed to generate noise random excitation in the spectrum 40–300 Hz. This study investigated the local behaviour of the window, and hence, lower frequencies were avoided as they involve global structure deformation or any other rigid body behaviour. The vibration was transmitted to the cabin lateral through a stinger as seen in Figure 1(b). An accelerometer was placed in the shaker's armature to record the excitation.

Two high-speed cameras, model Photron FastCam SA4 (1 megapixel full resolution), were employed to record the response on the inner surface of the window under excitation, as observed in Figure 2. Both cameras were supported on a rigid aluminium structure which was fixed to the bulkhead in order to isolate them from the vibration. The event was recorded at 2000 fps according to the Nyquist criterion and the shutter speed was 0.1 ms, short enough to avoid blurring. Two light sources were also employed to generate clear, high-contrast images. The accelerometer signal was synchronised with both cameras through a DAQ device model NI USB-6251.

(a) (b)

Figure 1: (a) Full-scale aircraft demonstrator and (b) the lateral excitation configuration using (i) a shaker with (ii) a stinger to measure on (iii) the passenger window.

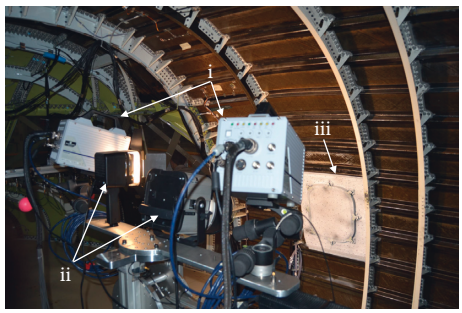

Figure 2: Stereoscopic setup composed by (i) two high-speed cameras and (ii) light sources recording on (iii) the passenger window from inside.

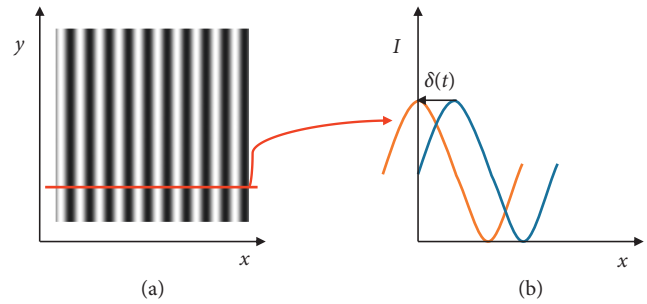

(a) (b)

Figure 3: (a) Sinusoidal fringe image and (b) the effect of x-motion in a 1D intensity profile.

Two additional forced normal mode tests were performed to validate the ODSs obtained from magnified images using the same setup and recording parameter as described in Figure 2.

3. Image Processing

3.1. Phase-Based Motion Magnification. In this study, the phased-based motion magnification methodology developed by Wadhwa et al. [7] was employed. This algorithm exploits the phase signals of the complex steerable pyramids, consisting in Gabor wavelets, at different positions and orientations to identify the local motions in spatial subbands of an image. The concept is analogous to Fourier shift theorem for sine function transforms. For instance, a generic 1D spatial-domain intensity profile, $I(x)$, that is moved according to a time-domain function, $\delta(t)$, can be described by a Fourier series decomposition as follows:

$$I(x+\delta(t)) = \sum_{\omega_s=-\infty}^{\infty} C_s e^{i\omega_s(x+\delta(t))}, \quad (1)$$

where ω_s is the frequency and C_s the amplitude of the sinusoid. Phase shifting of a hypothetical single sinusoid fringe image is shown in Figure 3 when motion occurs along the x direction. As can be observed, the phase is encoded as a phase shifting, $x + \delta(t)$, with respect to the initial position. Considering this analogy, the phase signal of each pyramid is then band-pass filtered and multiplied by a factor. The video reconstruction would show a magnified version of the motion present in that frequency band, previously imperceptible. Hence, the algorithm inputs are the image sequence, the desired frequency band, and the magnification factor.

For subsequent measurements using 3D-DIC, the sequence from each camera must be magnified using the same parameters [18]. Unlike sinusoidal excitation, many significant modes are now present in the images simultaneously. Therefore, magnification factors were chosen so that the responses of the nonmagnified modes were negligible in comparison with the magnified one.

Considering the random nature of the recorded vibration, the larger is the sequence, the better are the results. However, phase-based motion magnification is highly memory demanding, and this limits the sequence length. In this occasion, a computer with 32 GB RAM was employed allowing 1000 image sequences of 1 megapixel.

3.2. 3D Digital Image Correlation. Digital image correlation is an optical technique based on intensity field correlation to perform displacement and strain measurements in images [1]. For 3D-DIC, images from a stereoscopic system composed by using two cameras are employed. The calibration of the stereovision consisted in determining both extrinsic parameters, which define the relative position of the cameras and establish the relation of the coordinate systems, and intrinsic parameters, related to the position of the sensor, the lenses, and the light. An area of interest is identified in the

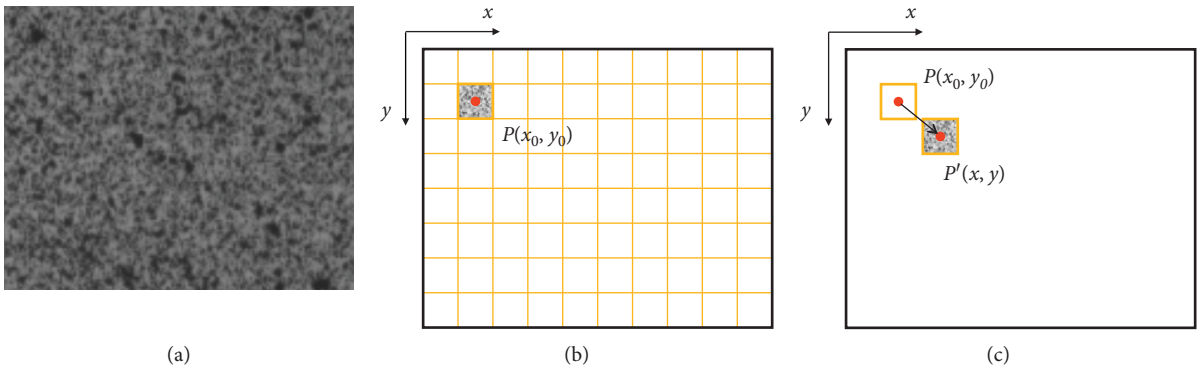

Figure 4: (a) Example of a grey-scale speckle pattern on the surface of interest. (b) Facet grid generation in the reference image highlighting that whose central pixel P. (c) Position of the pixel P after deformation, P′, to determine the displacement vector.

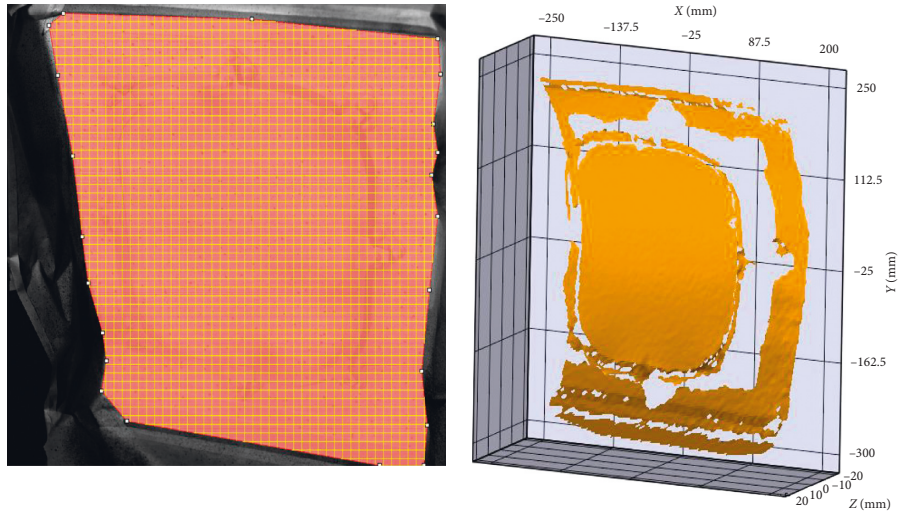

Figure 5: (a) Region of interest and facet size and (b) 3D digitalisation using 3D-DIC.

reference image from one camera and divided into squared subregions of pixels called facets or subsets. To make every facet unique, the surface is typically treated to generate a grey-scale speckle pattern as shown in Figure 4(a). The size of the facets is an odd number of pixels $(2M + 1)$, where M is an integer number, so that the facet central pixel is P at the position (x_0, y_0) [20], as shown in Figure 4(b). The central pixel of every facet is initially identified in the second camera as the most similar intensity area. With this first identification, it is possible to determine the spatial position of the central pixel of every facet, i.e., every measurement point and hence a digitalisation of the specimen surface. Performing the correlation in the subsequent deformed states, the displacement of every facet is determined, as shown in Figure 4(c).

In the present case, the window and the surrounding peel was coated with white paint and then sprayed with black paint to create the random speckle pattern. The correlation analysis was performed with Vic 3D software from Correlated Solutions Inc. using 19-pixel facet and 5-pixel overlap step. That generated a full-field measurement equivalent to 23000 3D sensors in this surface. Facet size can be compared with the image size in Figure 5(a), and the resulting surface digitalisation is shown in Figure 5(b).

4. Results and Discussion

As a broadband event, the expected response of the window to such excitation is a combination of the modes in this spectrum. Therefore, an instantaneous out-of-plane displacement, W, in Figure 6 shows that no clear mode shape extraction could be done by visualising the time-domain response. Actually, a significant amount of noise was also expected and found due to the low sensitivity of non-interferometric techniques in comparison with traditional pointwise sensors such as accelerometers or even laser vibrometry [21, 22]. Therefore, PMM was employed in this study to highlight individual ODSs, making both other modes and noise negligible [7, 14].

Before performing the magnification, some modes had to be identified. The full-field transfer functions were obtained from the 3D-DIC and the accelerometer measurements under the same noise excitation. The excitation

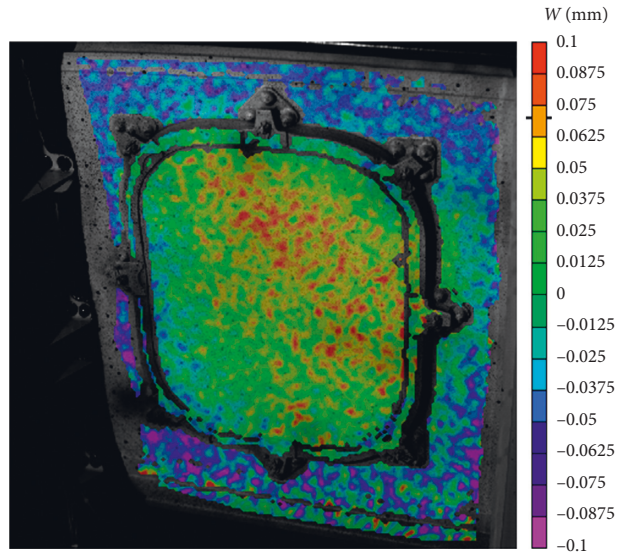

Figure 6: Instantaneous out-of-plane displacements, W, measured by 3D-DIC under random excitation.

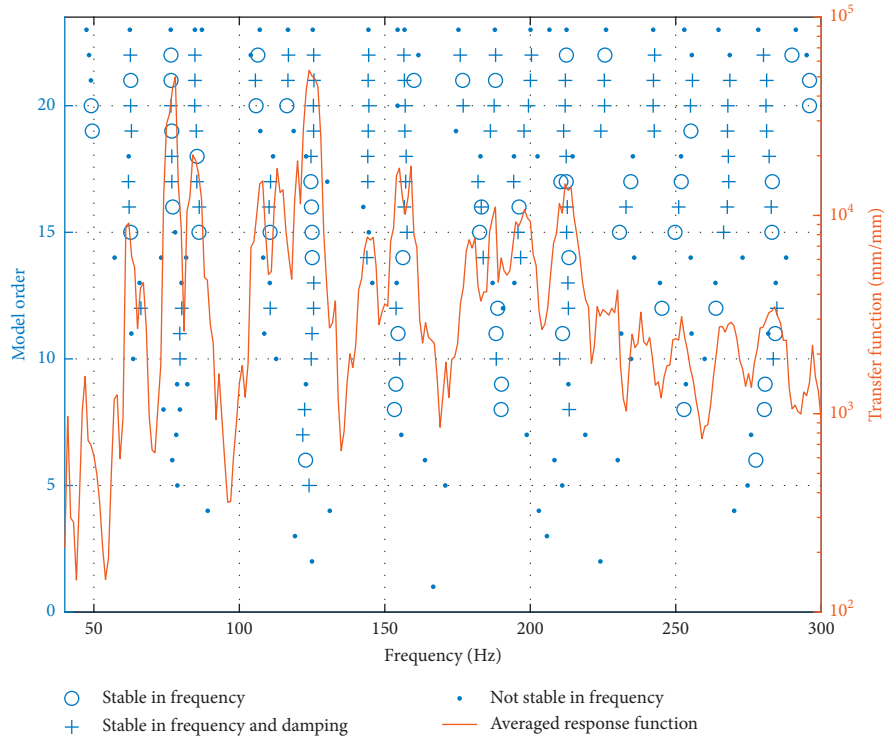

Figure 7: Stabilisation diagram obtained from the least squares complex exponential method applied to the full-field transfer functions.

displacement amplitudes were obtained by accelerometer signal double integration. As RAM was not a limitation for 3D-DIC processing but only for PMM, 5400 frame sequences were considered for this estimation that eventually yielded 1 Hz frequency resolution. The stabilisation diagram corresponding to the least squares complex exponential method was chosen to highlight modes. This diagram is represented in Figure 7 and shows the averaged transfer function. Multiple peaks were observed, many of which can be attributed to global structural modes that do not show the local behaviour of the region. These modes were not of interest in this study. The selected local modes for magnification were found at the peaks 124 Hz, 155 Hz, 215 Hz, and 268 Hz. In fact, these had the highest stabilisation trend and the selection is also supported by the previous study results [6]. Then, magnification was performed in a narrow band for each one. The magnification factors were 50x for 124 Hz and 100x for the rest. Those values were determined according to the level of response to yield clear displacement maps without producing blurring derived from excessive magnification.

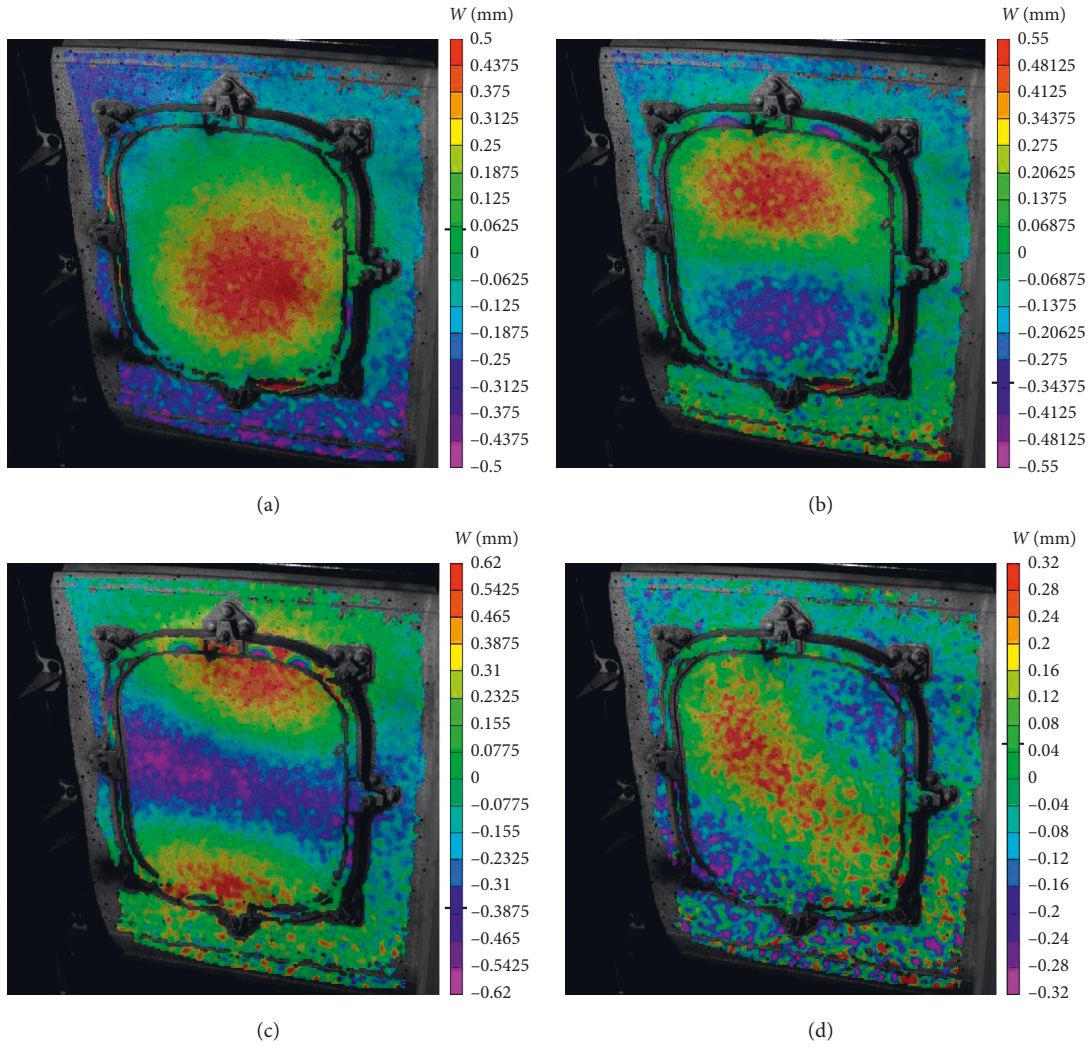

Figure 8: ODSs of the window in the out-of-plane direction, W, obtained with 3D-DIC after magnifying the resonances: (a) 124 Hz, (b) 155 Hz, (c) 215 Hz, and (d) 268 Hz.

As a result, videos were obtained showing a clear motion for the naked eye. The videos corresponding to the right-hand side camera can be found as Videos 1–4 in supplementary material for each respective mode. As can be seen, these videos describe the local behaviour of the window and the surrounding aircraft's peel. Comparing them, different deformations are noticed from one mode to another, and the complexity is increasing for higher frequency modes, as expected. This makes the interpretation of the motion difficult for the naked eye. Under this limitation, 3D-DIC measurements were performed in the magnified sequences. Taking into account that bending is mainly described by out-of-plane displacements, called as W, focus was placed on this direction. Four respective videos were obtained that included the displacement maps evolution (Videos 5–8). The instantaneous W maps at the signal crest are shown in Figure 8. The measurement allowed the quantification of the virtual motion of these images and improved the interpretation of the deformation. It is also worth mentioning the capabilities of the methodology to extract ODSs from a random event where just a combination of noise and modes was obtained. They all correspond to bending modes of increasing order mainly produced in the window itself. They can be checked against the ODSs obtained from forced normal mode tests. A quick identification of two resonances at 124 Hz and 215 Hz was performed with an impact hammer test. Hence, the ODSs for these frequencies under sinusoidal excitation are shown in Figure 9. Magnified ODSs from random tests show the same behaviour what proves they are actual ODSs and the influence of the remaining modes is negligible.

Overall, both sorts of video provide a meaningful insight of the behaviour of the window. For instance, the travelling wave effect produced by different phase lag along the surface is evidenced. For the first mode, the phase lag is more homogeneous, but this effect is especially relevant for the three higher frequency modes. However, there is an additional behaviour that might be of major importance for the integrity of the joint with the peel and hence for the air-tightness. In all the analysed resonances, the frame experienced deformation in certain zones with the highest amplitudes of the whole surface. By observing the displacement maps in Figure 8 (more notorious in Videos 5–8),

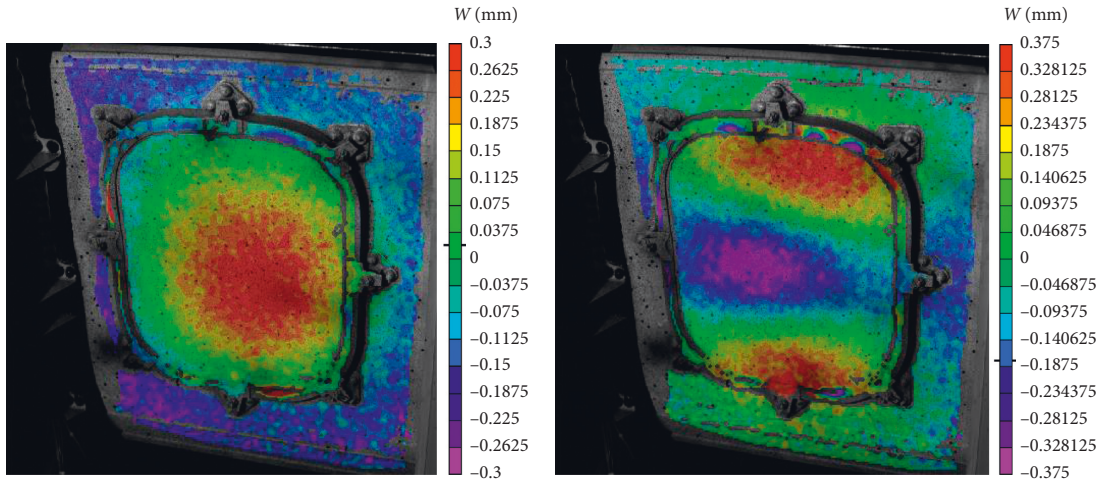

(a) (b)

Figure 9: ODSs of the window in the out-of-plane direction, W, obtained with 3D-DIC in forced normal mode tests for the resonances: (a) 124 Hz and (b) 215 Hz.

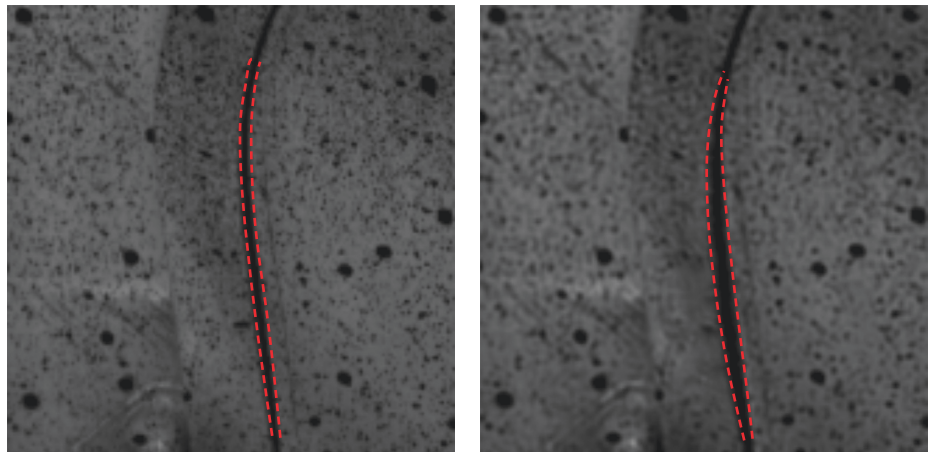

(a) (b)

Figure 10: Window's frame upper right corner in the nonloaded state (a) and at maximum deformation (b) for the magnified resonance 124 Hz.

this deformation can be localised. The motion may be intuited in the motion Videos 1–4, but zoom-in videos are provided for detailed inspection. In the first mode, large amplitudes are detected on the left part of the frame and also close to the right lower corner. They can be observed, respectively, in zoom-in Videos 9–10. Namely, the maximum deformation of the left part is compared with the nonloaded state in Figure 10. Blurring appeared in the frame as a consequence of the large displacements after magnification. Since the displacement in the window was smaller, the magnification factor was chosen to provide good displacement fields for the window despite the little blurring of the frame. As observed, maximum displacements for the second resonance mainly occur in the upper and lower parts, shown the former in Video 11. It is worthy to note that the third mode shows higher order deformation, especially close to the right upper corner as seen in Video 12. A particular case is the last mode as no deformation was detected in the frame in the W direction. However, vertical displacements, V, shown in Figure 11 revealed a significant deformation in the upper region of the frame. This vertical motion can be confirmed watching the zoom Video 13.

5. Conclusions

This study shows the benefits of the combination of phase-based motion magnification and 3D-DIC, especially for evaluating the complex structures where no conclusive information can be obtained from a single camera. Multiple ODSs of the passenger window of a full-scale aircraft demonstrator were deduced, visualized, and quantitatively measured from a single random excitation test. The magnification of an individual resonance from a broadband response makes it predominant against the other and its only

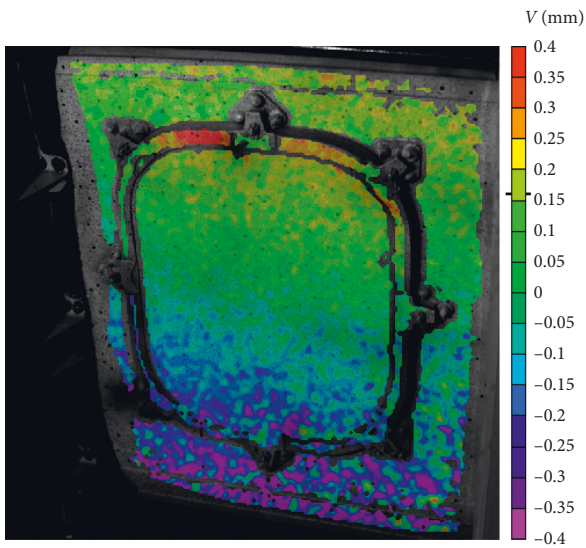

Figure 11: ODSs of the window in the vertical direction, V, obtained with 3D-DIC in forced normal mode tests for the resonance 268 Hz.

presence can be assumed. Larger amplitude motion achieved by magnification allowed clearer 3D-DIC displacement maps to be obtained which was little influenced by noise. On the contrary, 3D measurement provided the necessary information to understand the motion of the magnified videos. These measurements agreed with the ODSs obtained in forced normal mode tests. As a conclusion, visual and quantitative information proved to be complementary and provided a deep insight into an intuitive interpretation and understanding of the deformation.

Furthermore, this is a powerful tool for such big structures since it is able to give high-density information in critical parts which could not be achieved by using spaced sensors, being possible to lose localised effects. This paper has demonstrated the potential when detecting significant deformation of the window's frame. This provides relevant information and feedback to improve the union of the window and the peel that ensures the integrity and airtightness.

Data Availability

The data used to support the findings of this study are available from the corresponding author upon request.

Disclosure

Activities reported in this paper were developed in the frame of the European Community Seventh Framework Program, where Airbus Defence and Space S.A.U. was a partner of the Clean Sky Green Regional Aircraft Integrated Technology Demonstrator. The University of Jaén (Spain) participated under contract with Airbus Defence and Space S.A.U. in the field of testing technologies.

Conflicts of Interest

The authors declare that there are no conflicts of interest regarding the publication of this paper.

Supplementary Materials

A description of the videos supplied as supplementary materials is here provided. They can be found in the online version of the present paper.

Supplementary 1. Video 1: naked motion of the window ODS at 124 Hz using 50x magnification factor from the right-hand side camera viewpoint.

Supplementary 2. Video 2: naked motion of the window ODS at 155 Hz using 100x magnification factor from the right-hand side camera viewpoint.

Supplementary 3. Video 3: naked motion of the window ODS at 215 Hz using 100x magnification factor from the right-hand side camera viewpoint.

Supplementary 4. Video 4: naked motion of the window ODS at 268 Hz using 100x magnification factor from the right-hand side camera viewpoint.

Supplementary 5. Video 5: ODSs of the window in the out-of-plane direction, W, obtained with 3D-DIC after magnifying the resonance 124 Hz with 50x factor.

Supplementary 6. Video 6: ODSs of the window in the out-of-plane direction, W, obtained with 3D-DIC after magnifying the resonance 155 Hz with 100x factor.

Supplementary 7. Video 7: ODSs of the window in the out-of-plane direction, W, obtained with 3D-DIC after magnifying the resonance 215 Hz with 100x factor.

Supplementary 8. Video 8: ODSs of the window in the out-of-plane direction, W, obtained with 3D-DIC after magnifying the resonance 268 Hz with 100x factor.

Supplementary 9. Video 9: naked motion of the window ODS at 124 Hz using 50x magnification factor zooming at the left part of the frame from the right-hand side camera viewpoint.

Supplementary 10. Video 10: naked motion of the window ODS at 124 Hz using 50x magnification factor zooming at the right lower corner of the frame from the right-hand side camera viewpoint.

Supplementary 11. Video 11: naked motion of the window ODS at 155 Hz using 100x magnification factor zooming at the upper part of the frame from the left-hand side camera viewpoint.

Supplementary 12. Video 12: naked motion of the window ODS at 215 Hz using 100x magnification factor zooming at the upper part of the frame from the left-hand side camera viewpoint.

Supplementary 13. Video 13: naked motion of the window ODS at 268 Hz using 100x magnification factor zooming at the upper part of the frame from the left-hand side camera viewpoint.

References

[1] H. Schreier, J.-J. Orteu, and M. A. Sutton, *Image Correlation for Shape, Motion and Deformation Measurements*, Springer, Boston, MA, USA, 2009.

[2] R. Huňady and M. Hagara, "A new procedure of modal parameter estimation for high-speed digital image correlation," *Mech. Syst. Signal Process.*, vol. 93, pp. 66–79, 2017.

[3] D. A. Ehrhardt, M. S. Allen, S. Yang, and T. J. Beberniss, "Full-field linear and nonlinear measurements using continuous-scan laser Doppler vibrometry and high speed three-dimensional digital image correlation," *Mechanical Systems and Signal Processing*, vol. 86, pp. 82–97, 2017.

[4] P. L. Reu, D. P. Rohe, and L. D. Jacobs, "Comparison of DIC and LDV for practical vibration and modal measurements," *Mechanical Systems and Signal Processing*, vol. 86, pp. 2–16, 2017.

[5] T. J. Beberniss and D. A. Ehrhardt, "High-speed 3D digital image correlation vibration measurement: recent advancements and noted limitations," *Mechanical Systems and Signal Processing*, vol. 86, pp. 35–48, 2017.

[6] Á. Molina-Viedma, E. López-Alba, L. Felipe-Sesé, F. Díaz, J. Rodríguez-Ahlquist, and M. Iglesias-Vallejo, "Modal parameters evaluation in a full-scale Aircraft demonstrator under different environmental conditions using HS 3D-DIC," *Materials*, vol. 11, no. 2, p. 230, 2018.

[7] N. Wadhwa, M. Rubinstein, F. Durand, and W. T. Freeman, "Phase-based video motion processing," *ACM Transactions on Graphics*, vol. 32, no. 4, p. 1, 2013.

[8] E. P. Simoncelli, W. T. Freeman, E. H. Adelson, and D. J. Heeger, "Shiftable multiscale transforms," *IEEE Transactions on Information Theory*, vol. 38, no. 2, pp. 587–607, 1992.

[9] E. P. Simoncelli and W. T. Freeman, "The steerable pyramid: a flexible architecture for multi-scale derivative computation," in *Proceedings of the International Conference on Image Processing*, vol. 3, pp. 444–447, Washington, DC, USA, October 1995.

[10] J. Portilla and E. P. Simoncelli, "A parametric texture model based on joint statistics of complex wavelet coefficients," *International Journal of Computer Vision*, vol. 40, no. 1, pp. 49–70, 2000.

[11] H.-Y. Wu, M. Rubinstein, E. Shih, J. Guttag, F. Durand, and W. Freeman, "Eulerian video magnification for revealing subtle changes in the world," *ACM Transactions on Graphics*, vol. 31, no. 4, pp. 1–8, 2012.

[12] J. G. Chen, N. Wadhwa, Y.-J. Cha, F. Durand, W. T. Freeman, and O. Buyukozturk, "Modal identification of simple structures with high-speed video using motion magnification," *Journal of Sound and Vibration*, vol. 345, pp. 58–71, 2015.

[13] A. Sarrafi, Z. Mao, C. Niezrecki, and P. Poozesh, "Vibration-based damage detection in wind turbine blades using Phase-based Motion Estimation and motion magnification," *Journal of Sound and Vibration*, vol. 421, pp. 300–318, 2018.

[14] Y. Yang, C. Dorn, T. Mancini et al., "Blind identification of full-field vibration modes from video measurements with phase-based video motion magnification," *Mechanical Systems and Signal Processing*, vol. 85, pp. 567–590, 2017.

[15] Y. Yang, C. Dorn, T. Mancini et al., "Blind identification of full-field vibration modes of output-only structures from uniformly-sampled, possibly temporally-aliased (sub-Nyquist), video measurements," *Journal of Sound and Vibration*, vol. 390, pp. 232–256, 2017.

[16] Y. Yang, C. Dorn, T. Mancini et al., "Reference-free detection of minute, non-visible, damage using full-field, high-resolution mode shapes output-only identified from digital videos of structures," *Structural Health Monitoring*, vol. 17, no. 3, pp. 514–531, 2017.

[17] A. J. Molina-Viedma, L. Felipe-Sesé, E. López-Alba, and F. Díaz, "High frequency mode shapes characterisation using Digital Image Correlation and phase-based motion magnification," *Mechanical Systems and Signal Processing*, vol. 102, pp. 245–261, 2018.

[18] A. J. Molina-Viedma, L. Felipe-Sesé, E. López-Alba, and F. A. Díaz, "3D mode shapes characterisation using phase-based motion magnification in large structures using stereoscopic DIC," *Mechanical Systems and Signal Processing*, vol. 108, pp. 140–155, 2018.

[19] P. Poozesh, A. Sarrafi, Z. Mao, P. Avitabile, and C. Niezrecki, "Feasibility of extracting operating shapes using phase-based motion magnification technique and stereo-photogrammetry," *Journal of Sound and Vibration*, vol. 407, pp. 350–366, 2017.

[20] B. Pan, K. Qian, H. Xie, and A. Asundi, "Two-dimensional digital image correlation for in-plane displacement and strain measurement: a review," *Measurement Science and Technology*, vol. 20, no. 6, p. 062001, 2009.

[21] M. N. Helfrick, C. Niezrecki, P. Avitabile, and T. Schmidt, "3D digital image correlation methods for full-field vibration measurement," *Mechanical Systems and Signal Processing*, vol. 25, no. 3, pp. 917–927, 2011.

[22] C. Warren, C. Niezrecki, P. Avitabile, and P. Pingle, "Comparison of FRF measurements and mode shapes determined using optically image based, laser, and accelerometer measurements," *Mechanical Systems and Signal Processing*, vol. 25, no. 6, pp. 2191–2202, 2011.